International Journal of Numerical Methods for Heat & Fluid Flow

Natural convection from a heated T-open pipe of nanoencapsulated phase change material in a cavity

Ali Akremi
Department of Chemistry, College of Science, Northern Border University, Arar, Saudi Arabia

Mohammad Ghalambaz
Department of Mathematical Sciences, Saveetha School of Engineering, Saveetha Institute of Medical And Technical Sciences, Chennai, India, and Refrigeration and Air Conditioning Technical Engineering Department, College of Technical Engineering, The Islamic University, Najaf, Iraq

Ioan Pop
Department of Mathematics, Faculty of Mathematics and Computer Science, Babes-Bolyai University, Cluj-Napoca, Romania

Alin V. Rosca
Department of Statistics-Forecasts-Mathematics, Faculty of Economics and Business Administration, Babes-Bolyai University, Cluj-Napoca, Romania, and

Natalia C. Rosca
Department of Mathematics, Faculty of Mathematics and Computer Science, Babes-Bolyai University, Cluj-Napoca, Romania

Received 7 June 2025
Revised 13 August 2025
5 September 2025
Accepted 5 September 2025

Abstract

Purpose – This paper aims to study the natural convection from a heated T-open pipe of nanoencapsulated phase change material in a cavity. The impact of the presence of nanoencapsulated phase change materials (NEPCM) in water was studied on the thermal behavior of these novel nanoliquids in the presence of natural convection flows. The entropy generation for these nanoliquids was also investigated.

Design/methodology/approach – The NEPCM is modeled as a lumped phase change nanoparticle with a phase change material core and a polymer shell. The governing equations for a uniform mixture of NEPCM-water are written based on the conservation of mass, energy and also fluid motion. The natural convection effects were also taken into account. The finite element method was used to solve the governing equations. The entropy generation was also computed and studied.

Findings – Increasing the aspect ratio (AR) from 0.05 to 0.2 enhanced the average Nusselt number by 9%, while total entropy generation rose by 13%, indicating improved convective heat transfer near the bottom wall due to increased surface area. Enhancing the NEPCM nano particles volume fraction from 0 to 0.05 led to a 15% increase in heat transfer efficiency and a 9% rise in entropy, with negligible change in flow patterns. Growing the NEPCM fusion temperature from 0.1 to 0.5 slightly improved the Nusselt number by 5% and increased entropy by 3%, showing minor thermal gains with limited hydrodynamic impact.

Funding: The authors extend their appreciation to the Deanship of Scientific Research at Northern Border University, Arar, KSA for funding this research work through the project number NBU-FFR-2025-2246-10.

International Journal of Numerical Methods for Heat & Fluid Flow

0961-5539
DOI 10.1108/HFF-06-2025-0402

Practical implications – NEPCMs have demonstrated significant potential in heat and mass transfer for cooling systems and thermal energy storage. Encapsulation technology has been widely used to improve the stability, specificity and bioavailability of essential food ingredients, as well as the performance of NEPCM suspensions in cooling applications. Additionally, the NEPCM suspensions use the latent heat of nanoparticles and can effectively control surface temperatures.

Originality/value – The natural convection heat transfer and the entropy generation of NEPCM suspension are addressed in an enclosure with T-open heated walls for the first time.

Keywords Free convection, Nanoencapsulated phase change, Entropy generation, Finite element method

Paper type Research paper

1. Introduction

Heat transfer driven by natural convection within enclosed spaces plays a crucial role across many engineering applications, such as solar thermal systems, electronics temperature regulation and indoor climate control. The performance of these systems can be greatly improved by using fluids with superior thermal characteristics. In this context, nanoencapsulated phase change materials (NEPCMs) have gained attention as innovative thermal agents. These materials integrate the substantial heat absorption capacity of traditional phase change substances with the improved conductivity and structural stability provided by nanoscale encapsulation (Vemula and Öztop, 2024; Ghalambaz *et al.*, 2022; Reddy *et al.*, 2024).

The phase change materials (PCMs) are capable of storing or releasing substantial amounts of latent heat during phase transitions, such as from solid to liquid. This property makes them highly suitable for applications in thermal energy storage and temperature regulation. Despite their advantages, conventional PCMs face several challenges, including poor thermal conductivity, leakage during melting and a tendency to supercool – factors that hinder their effectiveness in real-world use (Vemula and Öztop, 2024; Reddy *et al.*, 2024). Nano-encapsulation addresses these limitations by encasing the PCM core within a stable shell material, typically polymeric (Ghalambaz *et al.*, 2022; Ghalambaz *et al.*, 2019). This core-shell structure not only prevents leakage and offers protection but also allows for the dispersion of PCM particles into a base fluid, forming a stable NEPCM suspension or nanofluid (Ghalambaz *et al.*, 2019; Reddy *et al.*, 2024). The resulting NEPCM suspension can then transport heat not only through sensible heat but also through the latent heat absorbed and released by the encapsulated PCM particles, significantly enhancing the overall heat transfer performance (Ghalambaz *et al.*, 2022). Common core materials include n-octadecane and n-nonadecane, while shells are often made of Polymethyl methacrylate (PMMA) or polyurethane (Vemula and Öztop, 2024; Wang *et al.*, 2024; Hidki *et al.*, 2024).

Natural convection, also known as free convection, occurs due to density variations within a fluid caused by temperature gradients. In an enclosure, these density differences lead to buoyancy forces, inducing fluid motion and subsequently transferring heat. The intensity of natural convection is primarily governed by the Rayleigh number (Ra), which represents the ratio of buoyancy forces to viscous forces (Ghalambaz *et al.*, 2019; Khedher *et al.*, 2024a; Khedher *et al.*, 2024b). Higher Rayleigh numbers generally indicate stronger convective flows and enhanced heat transfer. Other critical parameters include the Prandtl number (Pr), which relates momentum diffusivity to thermal diffusivity, and the Stefan number (Ste), which signifies the ratio of sensible heat to latent heat (Reddy and Sreedevi, 2024; Vemula and Öztop, 2024). For NEPCM suspensions, the fusion temperature of the encapsulated PCM plays a crucial role, as it dictates the temperature range at which latent heat storage and release occur (Reddy and Sreedevi, 2024; Raizah and Aly, 2022).

Numerous studies highlight the significant enhancement in heat transfer achieved by incorporating NEPCMs into base fluids for natural convection applications within enclosures. It has been consistently reported that NEPCM suspensions act as "smart working fluids" capable of significantly increasing average Nusselt numbers compared to pure fluids (Reddy *et al.*, 2024; Ghalambaz *et al.*, 2019; Wang *et al.*, 2024). This enhancement is primarily attributed to the latent heat absorption and release during the phase change of the encapsulated PCM cores. For instance, studies have shown that adding even a small volume fraction of NEPCM particles (e.g. 5%) can boost the heat transfer parameter by approximately 25% (Ghalambaz *et al.*, 2022). Similarly, a 5% volume fraction of NEPCMs can lead to a 12% increase in the time-averaged Nusselt number (Khedher *et al.*, 2024b), and 2% to 6% volume fraction can result in up to 20% enhancement (Reddy *et al.*, 2024). The optimal performance is often achieved at a specific range of nondimensional fusion temperatures, typically between 0.25 and 0.75 (Ghalambaz *et al.*, 2019; Khedher *et al.*, 2024b). The influence of NEPCM volume fraction on heat transfer is complex. While generally increasing the volume fraction enhances heat transfer, there might be an optimal range beyond which the cooling performance could deteriorate (Wang *et al.*, 2024). This could be due to increased viscosity or at higher concentrations, hindering fluid circulation.

The geometry of the enclosure and the heating configuration significantly impact the natural convection patterns and heat transfer rates. While the user specifically mentioned T-shaped heated plates, the provided articles explore various enclosure geometries and heating conditions, offering valuable insights that can be extrapolated. Studies involving square cavities with differentially heated vertical walls and insulated top/bottom walls are common benchmarks (Vemula and Öztop, 2024; Ghalambaz *et al.*, 2019; Wang *et al.*, 2024). Nonuniform heating, such as localized heating or nonuniformly heated boundaries, can induce complex flow patterns, including secondary recirculation eddies, which further influence heat transfer (Vemula and Öztop, 2024; Wang *et al.*, 2024). For example, a nonuniformly heated left vertical wall can lead to the formation of secondary recirculation near the upper left corner, expanding with increasing Rayleigh numbers (Vemula and Öztop, 2024).

The presence of internal obstacles or rotating elements within the enclosure adds another layer of complexity. Rotating superellipses inside a hexagonal cavity filled with NEPCM and porous media have been shown to augment temperature, concentration and streamline maximums, with the largest Nusselt and Sherwood numbers achieved for specific superellipse shapes (rhombus with convex and rectangle with rounded corners, respectively) (Raizah and Aly, 2022). Similarly, a rotating cold circular object within a trapezoidal porous enclosure filled with NEPCM enhances thermal transmission, especially at higher rotation speeds (Abderrahmane *et al.*, 2024a). The position of a rotating cylinder also plays a crucial role; for instance, positioning a cold rotating cylinder in the top section of a triangular cavity can lead to a substantial (240%) enhancement in the Nusselt number (Aissa *et al.*, 2024).

Wavy enclosures are also explored for their potential to enhance heat transfer due to increased surface area and flow mixing (Aly and Alsedais, 2025; Alhashash and Saleh, 2024; Aly and Alsedais, 2025). Studies on wavy star-shaped cavities with NEPCMs have shown that increasing amplitude and frequency parameters enhance thermal and concentration gradients and intensify oscillations in velocity and temperature fields, respectively (Aly and Alsedais, 2025). The corrugated number in wavy enclosures can also influence melting and solidification zones, with larger melting zones observed at moderate wave numbers (Alhashash and Saleh, 2024).

External factors like magnetic fields and mechanical vibrations can also be used to control and enhance heat transfer in nanofluids and NEPCM suspensions. Magnetohydrodynamics (MHD), which involves the interaction of electrically conducting fluids with magnetic fields,

is explored in several studies (Aly and Alsedais, 2025; Abderrahmane *et al.*, 2024a; Aissa *et al.*, 2024; Abderrahmane *et al.*, 2024b; Suchana and Molla, 2024; Reddy and Sreedevi, 2024; Ghalambaz *et al.*, 2024a). Magnetic fields generally suppress convective transport by inducing a Lorentz force that opposes fluid motion, thereby dropping peak velocity and mean Nusselt and Sherwood numbers (Aly and Alsedais, 2025; Abderrahmane *et al.*, 2024a; Abderrahmane *et al.*, 2024b; Suchana and Molla, 2024). Increasing the Hartmann number (Ha), which represents the ratio of magnetic force to viscous force, typically leads to a decrease in the Nusselt number (Abderrahmane *et al.*, 2024a; Suchana and Molla, 2024; Reddy and Sreedevi, 2024). This suppression of convection can be beneficial in certain applications where controlled or reduced flow is desired. For example, Alsedais *et al.* (2025b) numerically analyzed inclined MHD natural convection in a porous nanofluid cavity with gyrotactic microorganisms. Using the finite volume method, it explores the effects of heat source geometry, Peclet number, porosity and heat generation/absorption. Results show significant impacts on flow, heat transfer, entropy and microorganism distribution, validated via artificial neural networks.

Mechanical vibrations can actively enhance heat transfer in thermal systems. Studies on vibrational convection in NEPCM suspensions within porous enclosures show that the vibrational Rayleigh number has a strong impact, leading to a significant rise in the Nusselt number with higher vibration intensity (Khedher *et al.*, 2024a; Khedher *et al.*, 2024b). This highlights the potential of using active control mechanisms to optimize thermal performance.

Beyond heat transfer, mass transfer can also be a critical aspect, leading to double diffusion phenomena. Double diffusion convection, driven by combined temperature and concentration gradients, is relevant in various engineering scenarios. Studies involving NEPCMs in porous enclosures with double diffusion consider parameters like Lewis number (Le), Soret number (Sr) and Dufour number (Du) (Aly and Alsedais, 2025; Mourad *et al.*, 2025; Suchana and Molla, 2024; Alhejaili and Aly, 2024). Increasing Rayleigh and Darcy numbers notably enhances heat transfer rates in double diffusion scenarios, while the impact of Lewis number might be less pronounced (Mourad *et al.*, 2025). Soret and Dufour numbers, which represent thermodiffusion and diffusion-thermo effects, respectively, also influence the distributions of temperature, concentration and velocity fields (Aly and Alsedais, 2025; Alhejaili and Aly, 2024).

The behavior of NEPCM suspensions can also deviate from Newtonian fluid assumptions, especially at higher concentrations or under certain flow conditions. Research on power-law non-Newtonian NEPCMs in trapezoidal enclosures demonstrates that shear-thinning fluids (power-law index < 1) can exhibit higher local Nusselt and Sherwood numbers compared to Newtonian fluids (Suchana and Molla, 2024). This indicates that considering the non-Newtonian behavior of NEPCM suspensions is crucial for accurate predictions and optimization.

The increasing complexity of natural convection simulation of NEPCMs has led to the integration of machine learning (ML) models, particularly Artificial Neural Networks (ANNs), for enhanced predictive accuracy and understanding (Aly and Alsedais, 2025; Hidki *et al.*, 2024; Alhejaili and Aly, 2024). ML models can be trained on numerical simulation data to predict key performance metrics like average Nusselt and Sherwood numbers, offering a powerful tool for optimization and rapid analysis. For example, an eXtreme Gradient Boosting (XGBoost) (Alsedais *et al.*, 2025a) model has shown high accuracy in predicting average Nusselt and Sherwood numbers. An ANN model could achieve high *R*-squared values in predicting heat transfer characteristics of NEPCMs. The model was used in a porous square enclosure (Hidki *et al.*, 2024; Aly *et al.*, 2025) and a wavy porous cavity (Alsedais *et al.*, 2025a).

This synergy between numerical methods and machine learning is paving the way for more efficient design and analysis of NEPCM-based thermal systems.

The literature review shows that several heat and mass transfer aspects of nanoencapsulated phase change material, such as magnetohydrodynamic, double diffusive, mechanical vibrations, obstacles and rotating cylinders, have been investigated. However, the impact of internal heated walls on the heat and mass transfer of NEPCM suspensions has not been investigated. The current study aims to address the influence of internal hot T-shape walls on the natural convection flow and heat transfer of NEPCM suspensions for the first time.

2. Model description and mathematical formulation

The flow and heat transfer of NEPCMs in a cavity containing T-shape walls is investigated. As depicted in Figure 1, the top and bottom walls are insulated, while the left and right walls are at a cold temperature T_c. The geometry of the present study was selected following the study of Aly and Ahmed (2022) for the study of nanofluids. There are hot T-shaped plates at the middle. The nanoparticles are homogeneously dispersed in the water-based fluid and move with the fluid. The hot surface heats the nonliquid next to the hot plates, and the fluid moves upward until it reaches the cold layer, which loses its heat and moves downward. The nanoparticles are made of a phase change core and a polymer shell, as explained in Barlak *et al.* (2016). The core of nanoparticles undergoes a fusion process at a fusion temperature T_f Thus, a phase change area occurs in the enclosure. The nanoparticles move along with the fluid and lose their heat to cold regions and solidify again. The geometrical details of the model are explained in Figure 1. The NEPCM suspension is a homogeneous mixture of water and NEPCM particles. There is no aggregation, nanoparticle degradation or sedimentation. The phase change in nanoparticles is considered as a lumped effect, and there are no temperature or phase gradients in the nanoparticles.

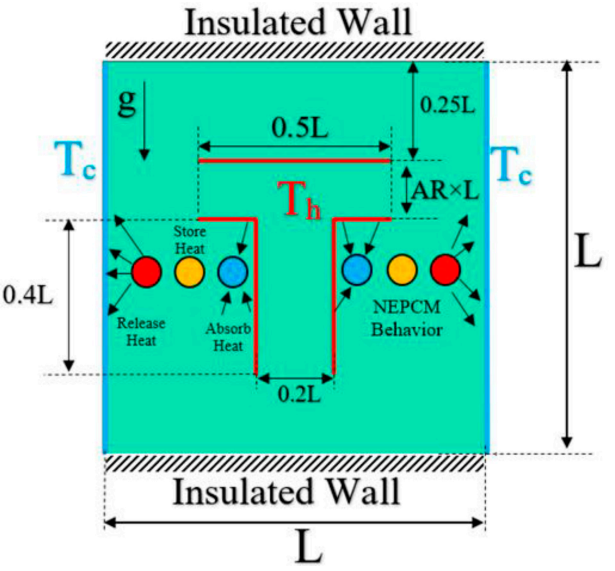

Figure 1. Schematic view of the physical model
Source: Authors' own work

The thermophysical characteristics of the core component (nonadecane), the base fluid (water) and the encapsulating layer (polyurethane) are detailed in Table 1. As per the reference in Barlak *et al.* (2016), nonadecane has a fusion temperature close to 32°C and a latent heat of approximately 211 kJ/kg.

2.2 Mathematical formulation

Considering a uniform distribution of NEPCM suspension, the governing equations for the (Ghalambaz *et al.*, 2019; Alazzam *et al.*, 2023).

Mass conservation:

$$\nabla^* u = 0 \tag{1}$$

Conservation of momentum:

$$\rho_{npcm}[(u.\nabla^*)u] = -\nabla^* p + \left(\mu_{npcm}\nabla^{*2}u\right) + f_B \tag{2}$$

Energy conservation:

$$(\rho Cp)_{npcm}[u.\nabla^* T] = k_{npcm}(\nabla^{*2}T) \tag{3}$$

where the buoyancy force ($\boldsymbol{f_B}$) is introduced as:

$$f_B = \begin{cases} x\text{: } 0 \\ y\text{: } \rho_{npcm}\beta_{npcm}g(T - Tc) \end{cases} \tag{4}$$

where the thermophysical properties are considered fixed, and the Boussinesq approximation was considered for the buoyancy forces. Here, ρ, Cp, β, k and μ indicate the density, heat capacity per unit of mass, thermal volume expansion, thermal conductivity and dynamic viscosity, respectively. The subscripts *npcm* and *Block* denote the suspension and solid wall. The gravity is represented by g. The field variables T and p denote the temperature and pressure, while u shows the velocity vector for suspension.

2.2 Physical relationships for the suspension

The density of the suspension is calculated through a weighted function incorporating both the dispersed nanoparticles and the host fluid (Chai *et al.*, 2018; Aly *et al.*, 2022). Here, subscripts np and f signify the nanoparticles and host fluid, respectively:

Table 1. Details the thermophysical attributes of the materials under consideration (Barlak *et al.*, 2016; Ghalambaz *et al.*, 2015)

Material	ρ (kg/m^3)	C_p (J/kg.K)	k (W/m.K)	β (K^{-1})	μ (kg/m.s)
Nonadecane	721	2,037	–	–	–
Polyurethane	786	1,317.7	–	17.28×10^{-5}	–
Host fluid (water)	997.1	4,179	0.613	21×10^{-5}	8.9×10^{-4}

Source(s): Authors' own work

$$\rho_{npcm} = \rho_f(1-\varphi) + \varphi\rho_{np} \tag{5}$$

For NEPCMs, the density can be computed using the following equation, where subscripts c and s correspond to the densities of the core and shell, respectively (see Chai *et al.*, 2018; Chen *et al.*, 2008):

$$\rho_{np} = \frac{\rho_s\rho_c(1+\iota)}{\rho_s + \rho_c\iota} \tag{6}$$

The weight ratio ι between the core and the shell for the materials under study is approximately 0.447 (see Barlak *et al.*, 2016). The heat capacity of the suspension is computed using the equation below (see Chen *et al.*, 2008; Khanafer and Vafai, 2011):

$$C_{p,npcm} = \frac{\rho_f C_{p,f}(1-\varphi) + \rho_{np} C_{p,np}\varphi}{\rho_{npcm}} \tag{7}$$

For the overall heat capacity and by considering the phase change in the nanoparticle core, a sinusoidal profile is proposed (see Chai *et al.*, 2018; Ghalambaz *et al.*, 2019; Ghalambaz *et al.*, 2024a):

$$C_{p,np} = C_{p,c} + \frac{\pi}{2}\left\{\left(\frac{h_{sf}}{\delta T} - C_{p,c}\right) sin\left(\pi\frac{T - T_{solid}}{\delta T}\right)\right\} \times \begin{cases} 0 & T < T_{solid} \\ 1 & T_{solid} < T < T_{liquid} \\ 0 & T > T_{liquid} \end{cases} \tag{8}$$

In this context, the temperature interval $\delta T = T_{liquid} - T_{solid}$ is defined as in which T_{liquid} and T_{solid} are the temperatures of the solid and liquid core nanoparticles. Here, $T_f = (T_{liquid} + T_{solid})/2$ is the phase change temperature of the nanoparticle's core. The suspension's volumetric thermal expansion coefficient is given by the following expression (Khanafer and Vafai, 2011):

$$\beta_{npcm} = \beta_f(1-\varphi) + \beta_{np}\varphi \tag{9}$$

The suspension's thermal conductivity and dynamic viscosity are determined using linear relationships, as shown below (see Zaraki *et al.*, 2015; Ghalambaz *et al.*, 2024a):

$$\frac{k_{npcm}}{k_f} = Nc\varphi + 1 \tag{10}$$

$$\frac{\mu_{npcm}}{\mu_f} = Nv\varphi + 1 \tag{11}$$

Here, N_v and N_c denote the numerical coefficients, which can be determined using experimental data such as those reported in Barlak *et al.* (2016).

2.3 Suspensions streamlines and entropy generation

The flow characteristics of the suspension can be illustrated using the contours of the streamlines (ψ). The streamlines are established based on the components of velocity, represented as:

$$u = \frac{\partial \psi}{y}, \; v = -\frac{\partial \psi}{\partial x} \tag{12}$$

and the streamline function is introduced as:

$$\nabla^{*2}\psi = \left(\frac{\partial u}{\partial y} - \frac{\partial v}{\partial x}\right) \tag{13}$$

Applicable boundary conditions for this equation are uniformly defined across all boundaries with zero streamline value. Entropy generation in the flow is influenced by two primary factors: thermal and frictional entropy. This is mathematically described by Ghalambaz *et al.* (2023) and Wang *et al.* (2024):

$$s_{local} = \frac{k_{npcm}}{T_0^2}\left[\left(\frac{\partial T}{\partial y}\right)^2 + \left(\frac{\partial T}{\partial x}\right)^2\right] + \frac{\mu_{npcm}}{T_0}\left(\left(\frac{\partial v}{\partial x} + \frac{\partial u}{\partial y}\right)^2 + 2\left(\left(\frac{\partial v}{\partial y}\right)^2 + \left(\frac{\partial u}{\partial x}\right)^2\right)\right) \tag{14}$$

In this equation, the first term represents entropy generation caused by temperature gradients, whereas the second term reflects entropy production resulting from viscous friction between fluid layers.

2.4 Applied boundary conditions

The isotherm temperatures of $T = T_c$ was applied at the side walls and $T = T_h$ at the inner T walls. The zero-heat flux was applied to the top and bottom walls. The zero velocity was applied to all walls exposed to the NEPCM suspensions. A zero-reference pressure was also considered at the bottom left corner of the enclosure in the fluid domain. Considering the model configuration and boundary conditions, a symmetric model about the central vertical axis could have been used. However, to maintain consistency with previous studies in the literature (Aly and Ahmed, 2022), the full model was adopted in the present work.

2.5 Dimensionless formulation

To render governing equations and the boundary conditions into dimensionless equations, the normalization parameters are introduced as (Reddy and Sreedevi, 2024; Ghalambaz *et al.*, 2019):

$$X = \frac{x}{L}, \; Y = \frac{y}{L}, \; \nabla^* = \frac{\nabla}{L}, \; l_1 = \frac{l}{L}, \; A = \frac{a}{L}, \; V = \frac{vL}{\alpha_f}, \; U = \frac{uL}{\alpha_f},$$

$$P = \frac{pL^2}{\rho_f \alpha_f^2}, \; \Psi = \frac{\psi}{\alpha_f}, \; \theta = \frac{T - Tc}{\Delta T}, \; \lambda = \frac{\Omega}{2\pi L} \tag{15}$$

and $\Delta = T_c - T_h$. This leads to the following dimensionless equations:

$$\nabla U = 0 \tag{16}$$

$$\frac{\rho_{npcm}}{\rho_f}[(U.\nabla)U] = -\nabla P + Pr\,\frac{\mu_{npcm}}{\mu_f}\nabla^2 U + F_B \tag{17}$$

$$Cr[U.\nabla\theta] = \frac{k_{npcm}}{k_f}(\nabla^2\theta) \tag{18}$$

where:

$$F_B = \begin{cases} X: 0 \\ Y: \dfrac{\rho_{npcm}}{\rho_f}\dfrac{\beta_{npcm}}{\beta_f} RaPr\,\theta \end{cases} \tag{19}$$

$$Cr = \frac{(\rho Cp)_{npcm}}{(\rho Cp)_f} = \lambda_0\varphi + \frac{\varphi}{Ste \times \delta} f + (1-\varphi) \tag{20}$$

$$f = sin\left(\frac{\pi}{\delta}\left(\theta + \frac{\delta}{2} - \theta_f\right)\right)\frac{\pi}{2} \times \begin{cases} 0 & \theta < \left(\theta_f - \dfrac{\delta}{2}\right) \\ 1 & \left(\theta_f - \dfrac{\delta}{2}\right) < \theta < \left(\theta_f + \dfrac{\delta}{2}\right) \\ 0 & \theta > \left(\theta_f + \dfrac{\delta}{2}\right) \end{cases} \tag{21}$$

and:

$$Pr = \frac{\mu_f}{\alpha_f \rho_f},\ Ra = \frac{\beta_f \rho_f \Delta T L^3 g}{\mu_f \alpha_f}, \tag{22}$$

$$\lambda_0 = \frac{(Cp_s\imath + Cp_{c,l})\rho_s\rho_c}{(\rho_c\imath + \rho_s)(\rho Cp)_f},\ \delta = \frac{\delta T}{\Delta T},\ Ste = \frac{(\rho_c\imath\rho_s)(\rho Cp)_f \Delta T}{(\rho_s\rho_c h_{sf})\alpha_f} \tag{23}$$

The density ratio $\rho_R = \rho_{np}/\rho_f = 0.7$ and $\rho_f = \rho_{npcm}/\rho_f = (1-\varphi) + \varphi \times \rho_R$.

The streamline and entropy generation are obtained as follows:

$$\nabla^2\Psi = \left(\frac{\partial U}{\partial Y} - \frac{\partial V}{\partial X}\right) \tag{24}$$

The dimensionless local entropy production (S_{Tlocal}) is expressed as:

$$S_T = \frac{k_{npcm}}{k_f}\left[\left(\frac{\partial\theta}{\partial Y}\right)^2 + \left(\frac{\partial\theta}{\partial X}\right)^2\right] + \chi_0\frac{\mu_{npcm}}{\mu_f}\left(\left(\frac{\partial U}{\partial Y} + \frac{\partial V}{\partial X}\right)^2 + 2\left(\left(\frac{\partial \mathrm{U}}{\partial X}\right)^2 + \left(\frac{\partial V}{\partial Y}\right)^2\right)\right) \tag{25}$$

where the irreversibility parameter (χ_0) is:

$$\chi_0 = \left(\frac{\alpha_f}{\nabla T \times L}\right)^2 \frac{T_f \mu_f}{k_f} \tag{26}$$

2.6 Heat transfer rate and total entropy generation

The heat transfer rate at the hot wall is characterized by the local Nusselt number as:

$$Nu_Y = -\frac{k_{npcm}}{k_f}\left(\frac{\partial\theta}{\partial X}\right)_{X=0} = -(1 - Nc\phi)\left(\frac{\partial\theta}{\partial X}\right)_{X=0} \tag{27}$$

$$Nu_{avg} = \int_0^1 Nu_Y\, dY \tag{28}$$

$$S_T = \iint_A s_{T,local} dA \tag{29}$$

where A is the surface area of the domain.

3. Solution method and verification

3.1 Numerical method

Galerkin's weighted finite element method was deployed to numerically address the dimensionless governing equations – namely, equations (17)–(20). The computational domain was discretized using an unstructured mesh, with a particular focus on grid density in regions adjacent to solid boundaries. This was done to accurately capture rapid changes in both velocity and temperature profiles. To ensure full coupling of the discretized governing equations, the damped Newton method was applied. A damping value of 0.8 was applied for better convergence. The ensuing system of linear algebraic equations was then solved through the use of the Parallel Sparse Direct Solver. The computations were halted when the relative error reached below 10^{-4}. For a comprehensive explanation of the numerical methods used, please refer to Zienkiewicz *et al.* (2014). After the computation of the flow field and temperature field, the entropy generation field and heat transfer at the walls were calculated. A continuous approach for the study of a range of parameters was applied. In this approach, as the value of a control parameter changes step by step, the solution for a parameter at a previous step was used as an initial guess for the next step.

3.2 Code validation and grid independence process

An unstructured mesh incorporating boundary-layer meshes at the walls was used for discretizing the governing equations and performing numerical computations. A mesh sensitivity study was conducted to evaluate how mesh resolution affects result accuracy. For this investigation, a representative scenario $AR = 0.15$, $\varphi = 0.05$, $\mathrm{Ra} = 1e^4$, $\theta_f = 0.3$, $\mathrm{Pr} = 6.2$, $Nc = Nv = 6$, $\mathrm{Ste} = 0.3$, $X_0 = 1E\text{-}4$ was chosen, and simulations were run across various mesh densities as detailed in Table 2.

The simulation outcomes, illustrated in Figure 2, demonstrate minor variations attributed to changes in mesh size. It was impossible to further reduce mesh resolution, as coarser meshes resulted in solution divergence. Hence, considering the balance between computational expense, accuracy and the need to prevent divergence, the mesh designated as Case No. 4 was selected for subsequent simulations. Figure 3 provides a visualization of the chosen mesh configuration.

3.3 Validation and code verification

To substantiate the numerical accuracy of the finite element code used in this study, comparisons have been made between the results obtained here and those published in prior

Table 2. Impact of mesh elements on average Nusselt number

Case no.	Mesh quality	Mesh quantity (overall number of elements)	Nu_t	*Err* (%)
1	Normal	1,554	4.5082	1.22
2	Fine	2,509	4.4539	0.71
3	Finer	6,559	4.4226	0.21
4	Extra fine	17,218	4.4134	0.33
5	Extremely fine	25,973	4.3990	–

Source(s): Authors' own work

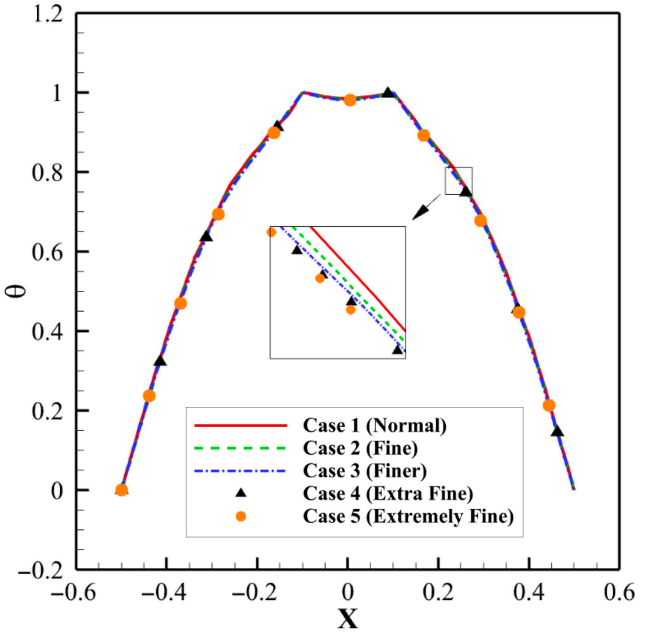

Figure 2. Temperature at middle line of the enclosure at $Y = 0$ for various evaluated meshes
Source: Authors' own work

works (see Kahveci, 2010; Turan *et al.*, 2011; Ilis *et al.*, 2008; Calcagni *et al.*, 2005). Table 3, as well as Figures 4 and 5, showcase these comparative analyses. Specifically, Table 3 contrasts the average Nusselt numbers from this study with those presented in reference Kahveci (2010). The latter work explored buoyancy-driven convective flow inside a square cavity loaded with water-TiO_2 nanoparticle suspension featuring isothermally heated vertical walls and insulated horizontal walls.

For additional verification, the temperature profiles generated by our numerical code for fluid flow in a square enclosure are compared against the results of the study of Turan *et al.* (2011) as illustrated in Figure 4. Furthermore, Figure 4 plots the entropy fields of the present work alongside those presented in Ilis *et al.* (2008).

Figure 5 provides a comparison between our results and those published in Ghalambaz *et al.* (2019) for an NEPCM suspension when $Ra = 10^5$, $\theta_f = 0.3$, $Pr = 6.2$, $St = 0.3$,

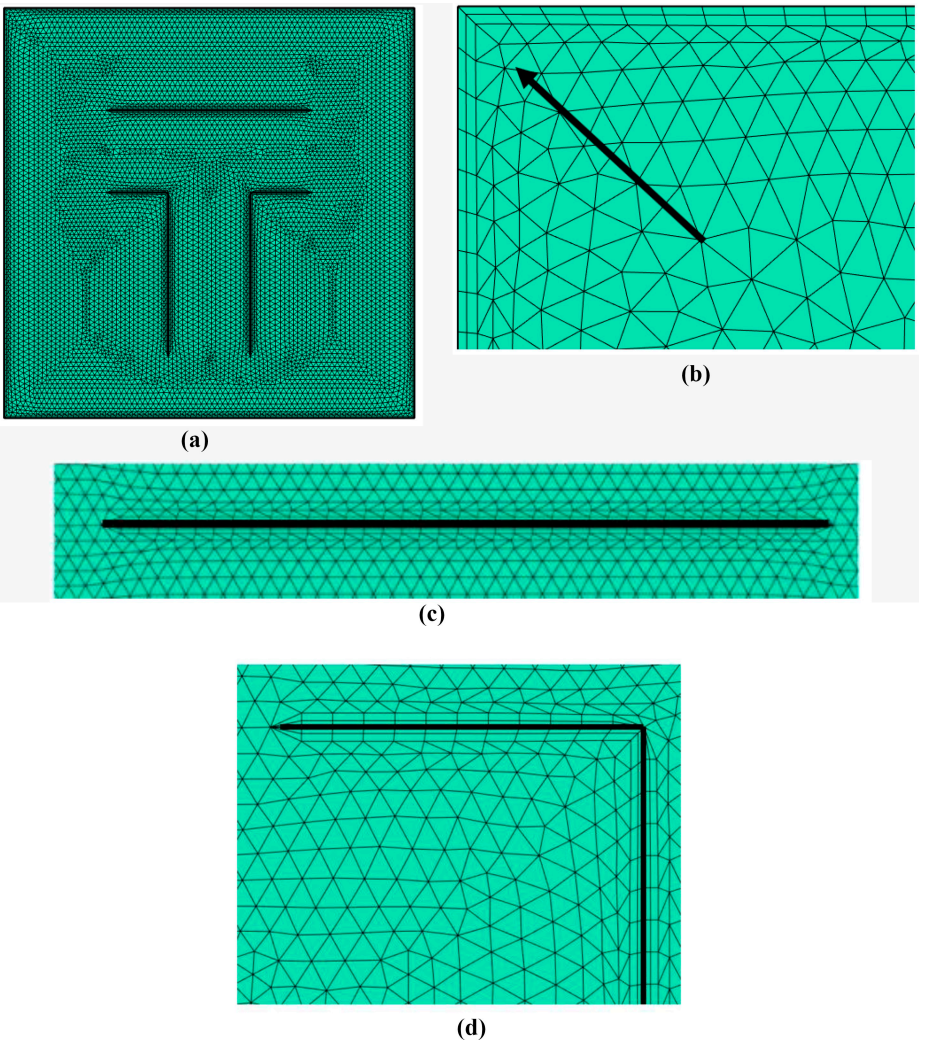

Figure 3. Views of the chosen grid size (Case 4 with extra fine quality), (a) overall view, (b) a zoomed view on the left-top corner of the enclosure, (c) close to the top horizontal wall and (d) close to the corner of the bottom wall

Source: Authors' own work

Table 3. Results of Kahveci (2010) and current research for average Nusselt number $(Ra = 10^6)$

$Nu_{average}$	$\varphi = 0.0$	$\varphi = 0.05$	$\varphi = 0.1$
Kahveci (2010)	9.23	9.77	10.23
Current research	9.20	9.76	10.30

Source(s): Authors' own work

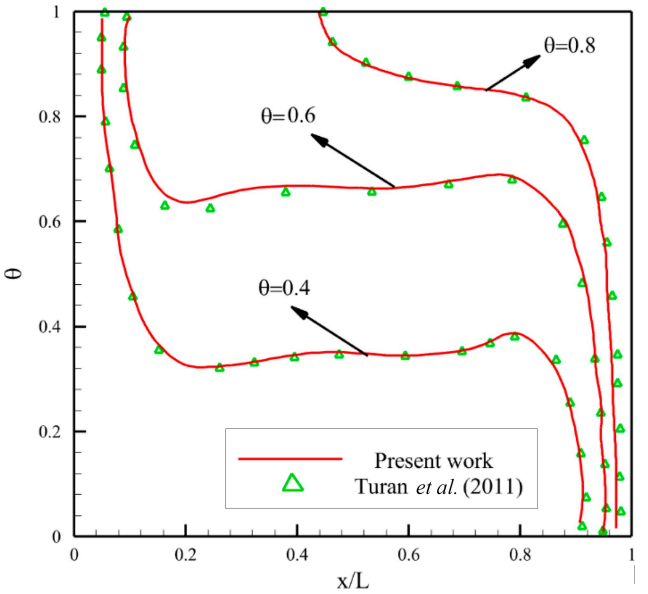

Figure 4. Isotherms evaluated in our study and those obtained by Turan *et al.* (2011)
Source: Authors' own work

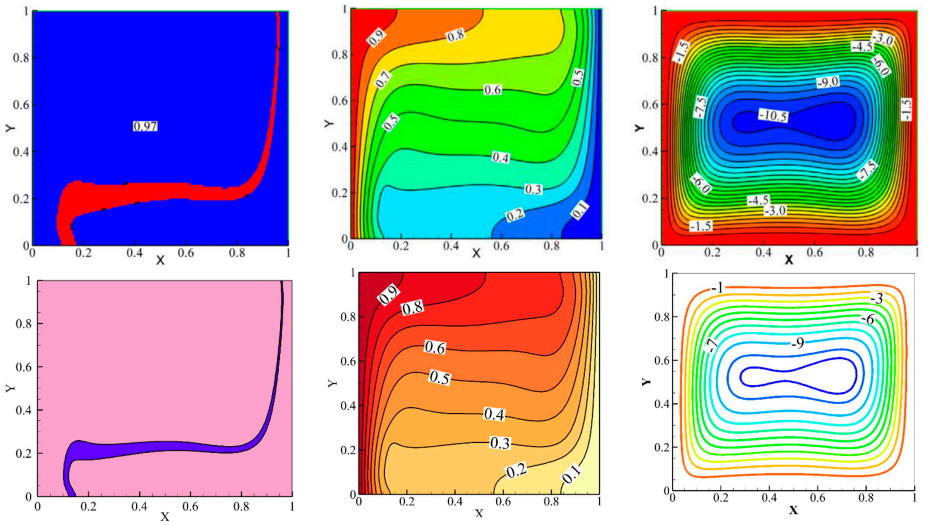

(a) CR contours (b) Isotherms (c) Streamlines

Figure 5. Comparison between the *CR*, isotherms and streamlines of the present study and those by Ghalambaz *et al.* (2019) for heat transfer of NEPCM suspensions in a square cavity
Source: Authors' own work

$\lambda_0 = 0.33$, $N_v = 3$, $N_c = 3$ and $\varphi = 0.05$ and $\rho_p/\rho_f = 0.9$. The isotherms, phase transition (Cr) maps, and streamlines are compared. As seen, a good match between the results can be found. Additionally, a comparative analysis was conducted between the findings of reference Ghalambaz *et al.* (2024b) and the current simulations on heat transfer involving two square cylinders in Figure 6. In this setup, the outer vertical walls were maintained at cold temperatures, while the left inner vertical wall was heated. The remaining walls were insulated. The aspect ratio (L) of the cylinders was set at 0.3.

4. Results and discussion

The default values for the first paragraph of the section: $AR = 0.15$, $\varphi = 0.05$, $Ra = 1e4$, $\theta_f = 0.3$, $Pr = 6.2$, $Nc = Nv = 6$, $Ste = 0.3$, $X_0 = 1e\text{-}4$. Here, the impact of $0.05 < AR < 0.2$, $0 < \varphi < 0.05$, $1e1 < Ra < 5e4$ and $0.1 < \theta_f < 0.9$ on the phase change flow and heat transfer is addressed.

Figure 6 illustrates the local Nusselt number distribution along the left cold wall. Figures 7–10 depict the isotherms, heat capacity ratio (Cr) maps, streamlines and entropy generation field for various AR values. The change of wall geometry due to the change of AR is evident in these figures. As AR increases, the distance between T-shaped walls increases, and the bottom hot wall moves downward.

From Figure 6, it can be observed that increasing the aspect ratio (AR) leads to a rise in the local Nusselt number at the lower section of the cold wall. However, changes in AR have minimal influence on the local Nusselt number (Nu_Y) near the upper section. This behavior occurs because an increase in AR extends the length of the T-shaped walls downward, enlarging the heated surface area near the bottom. Consequently, the cavity temperature in

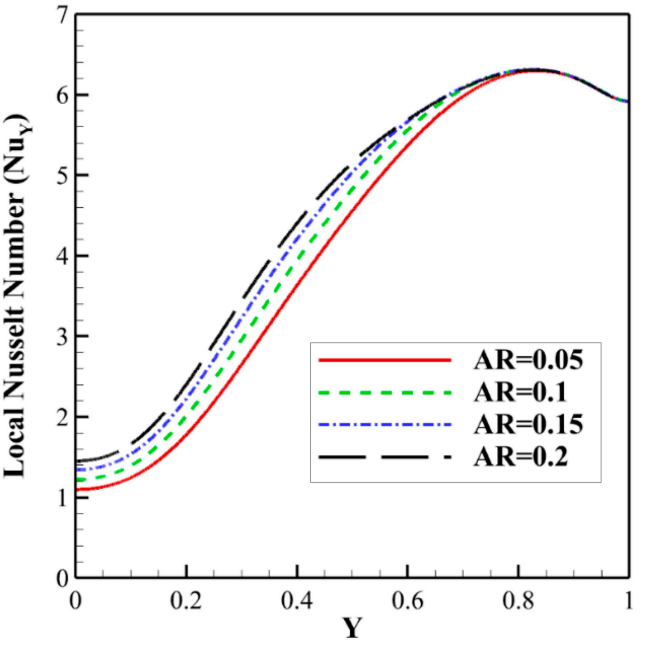

Figure 6. Local Nusselt number as a function of aspect ratio (AR) parameter
Source: Authors' own work

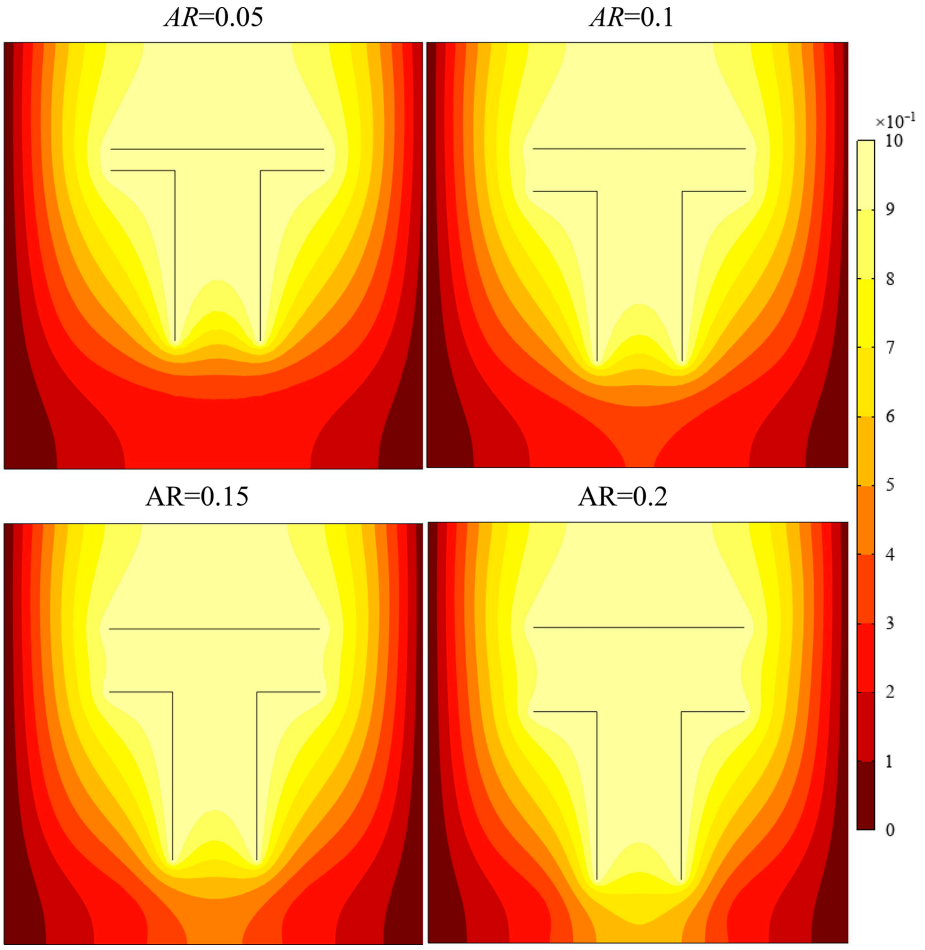

Figure 7. Influence of aspect ratio (AR) on temperature contours
Source: Authors' own work

these lower regions increases, enhancing the local heat transfer, as indicated by the higher Nusselt number.

As the NEPCM fluid rises along the wall, its temperature gradually decreases, resulting in reduced temperature gradients. This decrease in temperature gradient eventually diminishes the beneficial effect of the expanded surface area located in the lower regions of the wall, rendering the influence on the Nusselt number (NuY) negligible in the upper sections. Isotherms illustrate low-temperature regions adjacent to the cold walls, whereas the region immediately above the T-shaped walls remains relatively hot due to free convection effects. With a rise in the aspect ratio (AR), the upper region next to the cold walls experiences a temperature rise, thereby increasing the local Nusselt number, as plotted in Figure 6.

An elevation in AR causes the crystallization (Cr) maps to shift downward, as presented in Figure 8. These Cr maps identify regions undergoing NEPCM phase transitions. When the hot

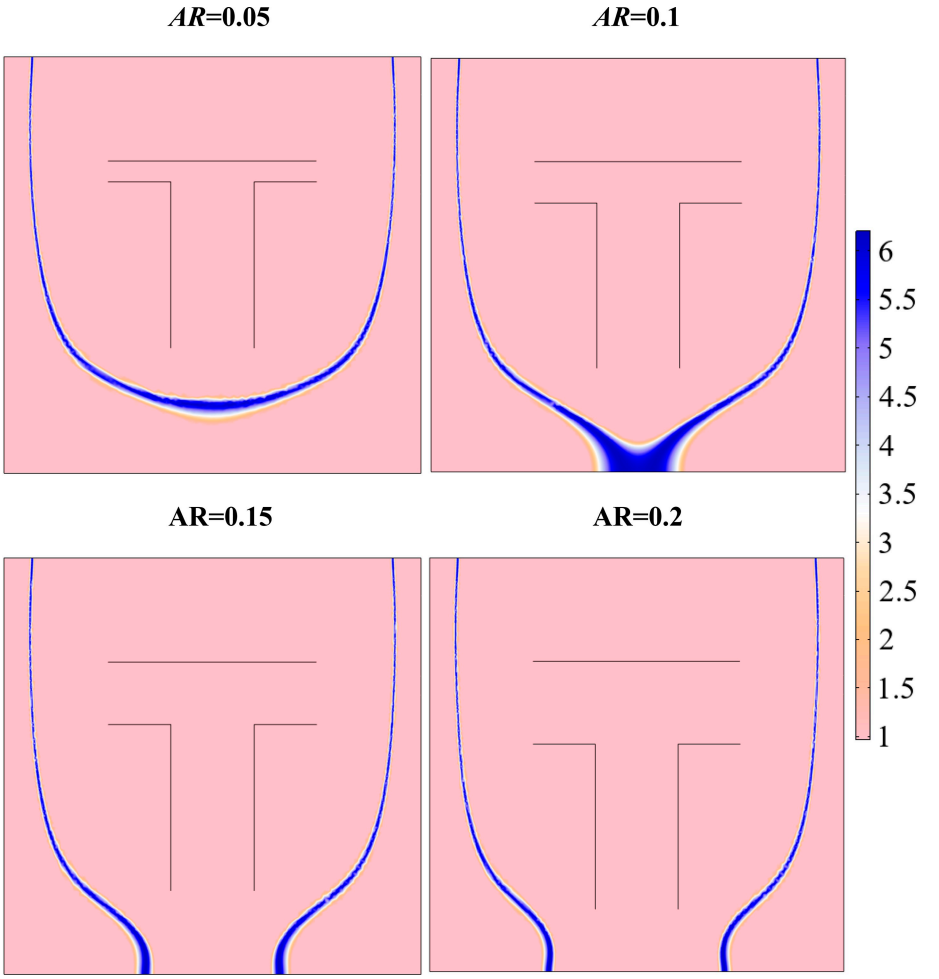

Figure 8. Influence of aspect ratio (*AR*) on phase transition maps
Source: Authors' own work

walls move downward, the high-temperature isotherms (close to the fusion temperature) shift accordingly toward the bottom, approaching the cold walls more closely. Figure 9 reveals a distinct zone of elevated entropy generation concentrated along the edges of the lower hot walls. This localized intensification is primarily driven by the coexistence of steep temperature gradients and pronounced velocity variations in these regions. As the incoming NEPCM suspension – initially at a relatively low temperature – comes into direct contact with the hot wall surfaces, it experiences rapid thermal transitions. The abrupt heat transfer in this region significantly enhances local irreversibilities, thereby amplifying entropy generation.

A secondary but noteworthy contribution to entropy generation is observed near the outer ends of the horizontal hot walls. In these peripheral areas, the interaction between the NEPCM flow and the heated surfaces remains significant, but the intensity of entropy

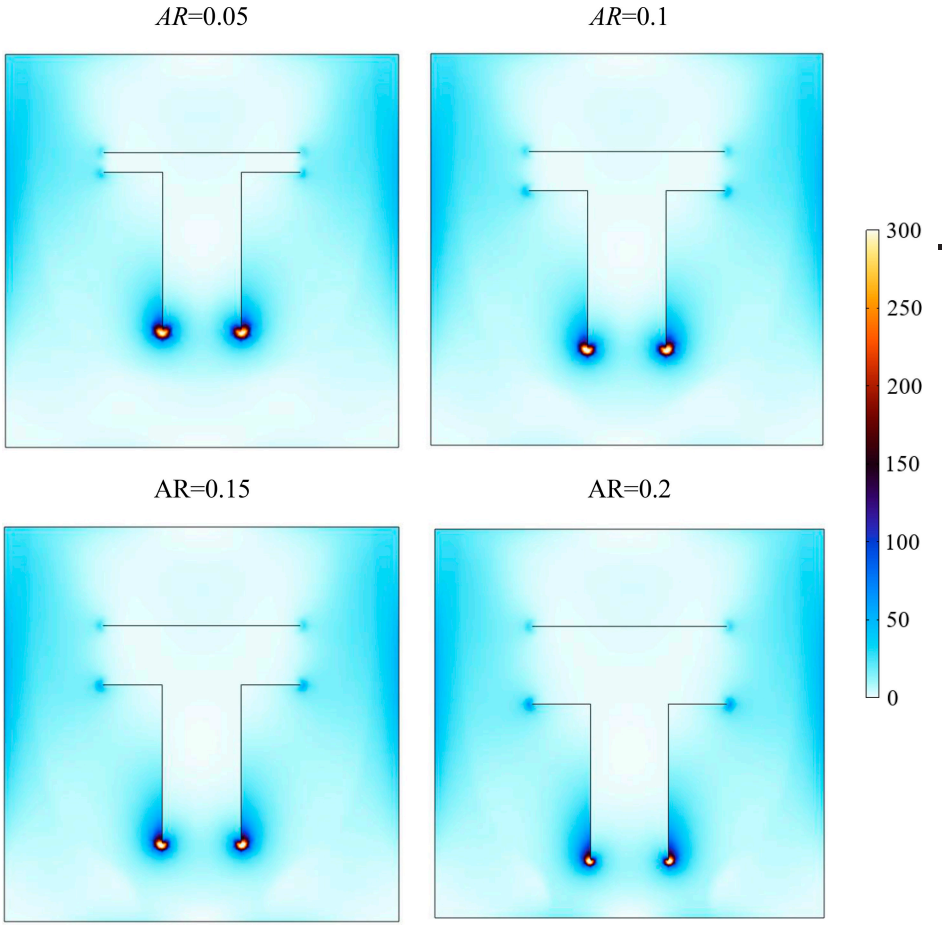

Figure 9. Influence of aspect ratio (*AR*) on entropy generation contours
Source: Authors' own work

production is comparatively diminished. This reduction stems from the fact that the NEPCM has already undergone substantial preheating while passing over the lower hot wall sections. As a result, the local temperature gradients become less severe, and the associated velocity field variations are smoother, leading to more moderate entropy generation rates and a less abrupt spatial distribution of irreversibilities in these zones.

The streamlines are plotted in Figure 11. There are two separate circulation regions in the enclosure. As *AR* rises and the gap between the hot walls widens, the circulation regions also enter the space between the hot walls. Thus, the inner surface of the hot walls also contributes to the convection heat transfer. There is not much of NEPCM fluid circulation at the top region since that region is already hot, and a semi-stratified space has formed (see Figure 7).

Figure 11 illustrates the local Nusselt number distribution for various Ra values. The corresponding temperature fields (isotherms), crystallization (*Cr*) maps, entropy generation patterns and streamlines are presented in Figure 12. Figure 11 showed that a growth in the Ra

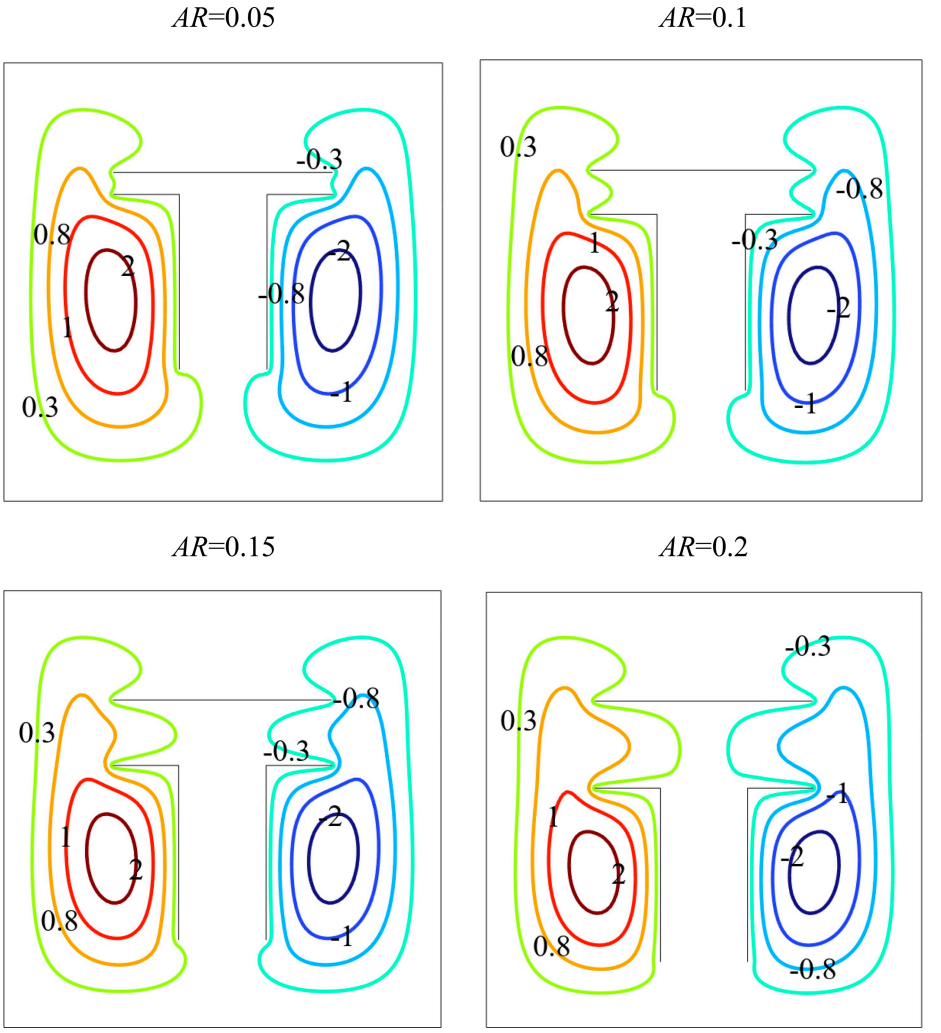

Figure 10. Influence of aspect ratio (*AR*) on streamlines
Source: Authors' own work

generally enhances the local Nusselt number. This enhancement arises from improved natural convection and more vigorous fluid circulation.

However, the impact of varying the Rayleigh number on the local Nusselt number (Nu_Y) at the lower portion of the cold wall does not exhibit a monotonic trend. At lower Rayleigh numbers (e.g. $Ra = 1 \times 10^3$), natural convection effects are relatively weak, as indicated by the streamline patterns in Figure 12. Under these conditions, heat transfer is predominantly conductive.

As the Rayleigh number increases, significant distortion of isotherms occurs, notably around the sharp edges of the lower hot walls. Simultaneously, the region characterized by

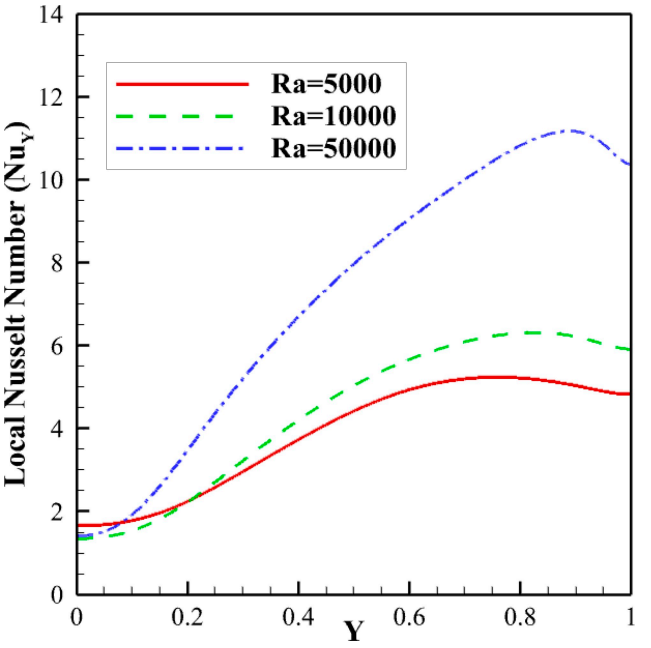

Figure 11. Local Nusselt number as a function of Rayleigh number
Source: Authors' own work

elevated temperatures and stratified warm NEPCM suspension expands near the top. Interestingly, an increase in Rayleigh number also reshapes and relocates the *Cr* maps toward the lower central region. These *Cr* maps typically align along an isotherm near the fusion temperature. Thus, as the isotherms concentrate around the hot walls at the bottom, the *Cr* maps also reposition into these concentrated regions.

Elevating the Rayleigh number intensifies entropy generation at the sharp edges of the lower hot walls and adjacent to the cold walls. Particularly high entropy generation occurs in the midsection of the cold walls, as depicted in Figure 12. This pattern emerges due to the NEPCM flow circulating around the hot walls positioned slightly above the insulated bottom boundary. Furthermore, the presence of a stratified hot region near the top reduces fluid velocity and heat transfer, creating conditions that elevate temperature gradients and subsequently increase the entropy generation rate at the middle portion of the cold walls.

Figure 13 illustrates the influence of NEPCM particle concentration on the local Nusselt number (Nu_Y), with corresponding contour maps presented in Figure 14. An increase in the concentration of NEPCM particles generally enhances the local Nusselt number. This enhancement occurs due to improved thermal conductivity and higher effective heat capacity, primarily arising from the latent heat fusion associated with nanoparticles. While an increase in NEPCM particle concentration slightly reduces temperature gradients due to the enhanced thermal properties, it concurrently improves overall heat transfer, leading to higher local Nusselt numbers. Figure 14 reveals that higher NEPCM concentrations broaden the crystallization (*Cr*) regions slightly. This phenomenon is attributable to increased thermal conductivity, resulting in smoother temperature gradients across the fluid domain. Additionally, raising the NEPCM particle concentration modestly increases entropy

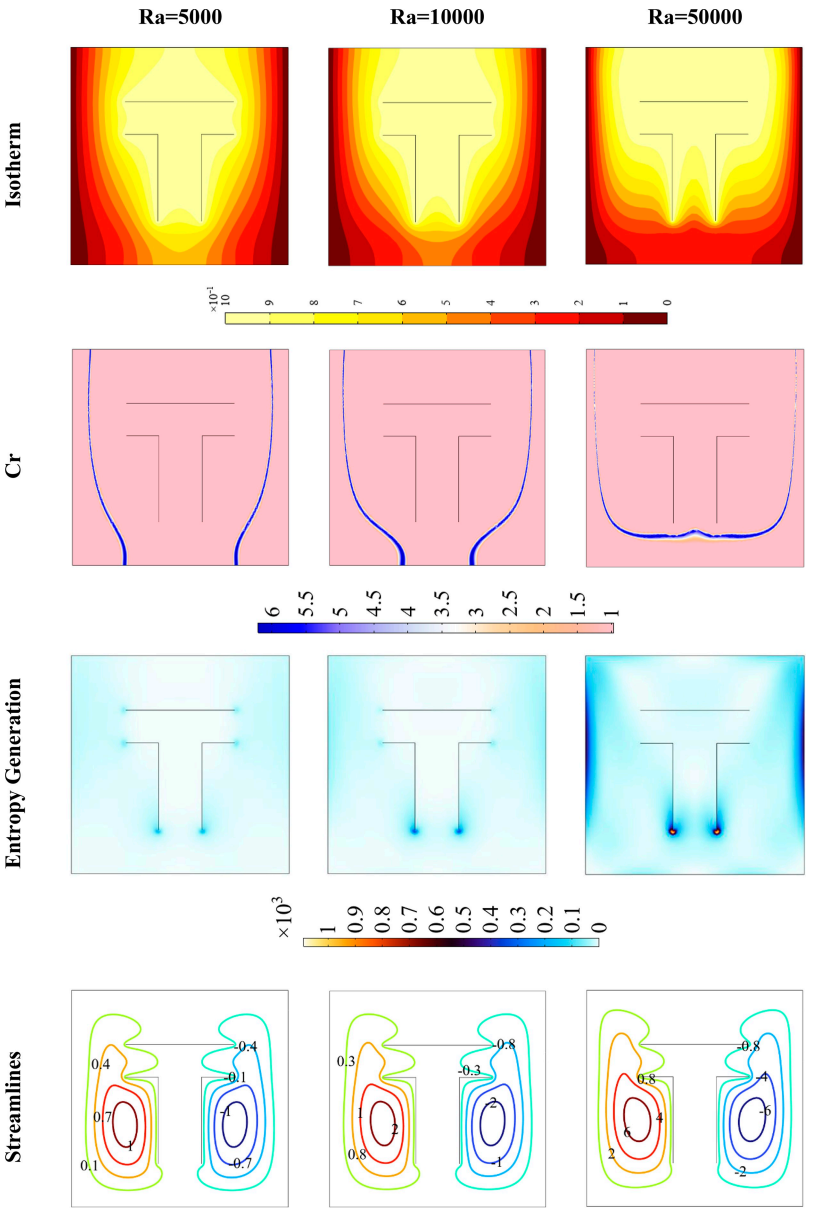

Figure 12. Influence of Rayleigh number (Ra) on (First row) Isotherm contour, (Second row) *Cr*, (Third row) Entropy generation and (Forth row) streamlines
Source: Authors' own work

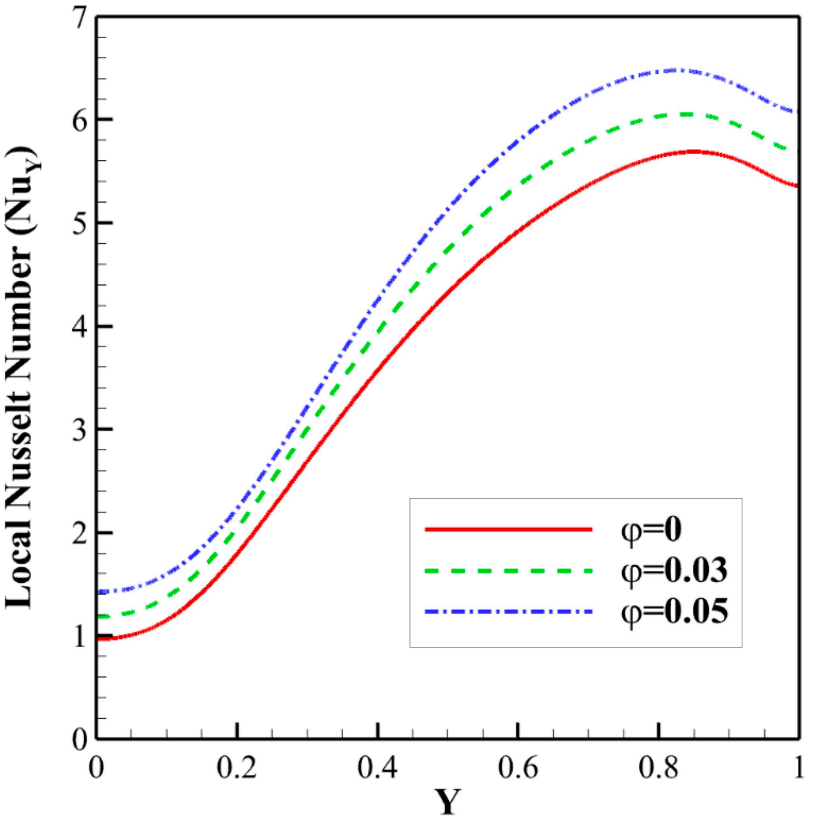

Figure 13. Local Nusselt number as a function of volume fraction of the nanoparticles
Source: Authors' own work

generation within the system. Entropy generation notably intensifies at the sharp edges of the hot walls, driven primarily by enhanced overall heat transfer rates. However, changes in NEPCM particle concentration have minimal effects on streamline patterns, suggesting a negligible impact on the fundamental fluid flow behavior.

Figure 15 presents the influence of NEPCM particle fusion temperature on Nu_Y, with the corresponding contour maps displayed in Figure 16. An increase in the fusion temperature leads to an enhancement of the local Nusselt number, indicating improved heat transfer performance. As the fusion temperature rises, the phase transition zone shifts next to the hot walls (refer to Figure 16). This repositioning enhances the local temperature gradients, as the phase transition region resists temperature changes and facilitates greater heat absorption due to latent heat effects, thereby improving the overall heat transfer rate. Furthermore, increasing the fusion temperature elevates the entropy generation, particularly near the sharp edges of the hot walls, which correlates directly with the intensified heat transfer in these areas. Notably, the variation in fusion temperature produces minimal changes in the streamline patterns and the natural convection circulation within the domain, indicating that the dominant effects are thermal rather than hydrodynamic.

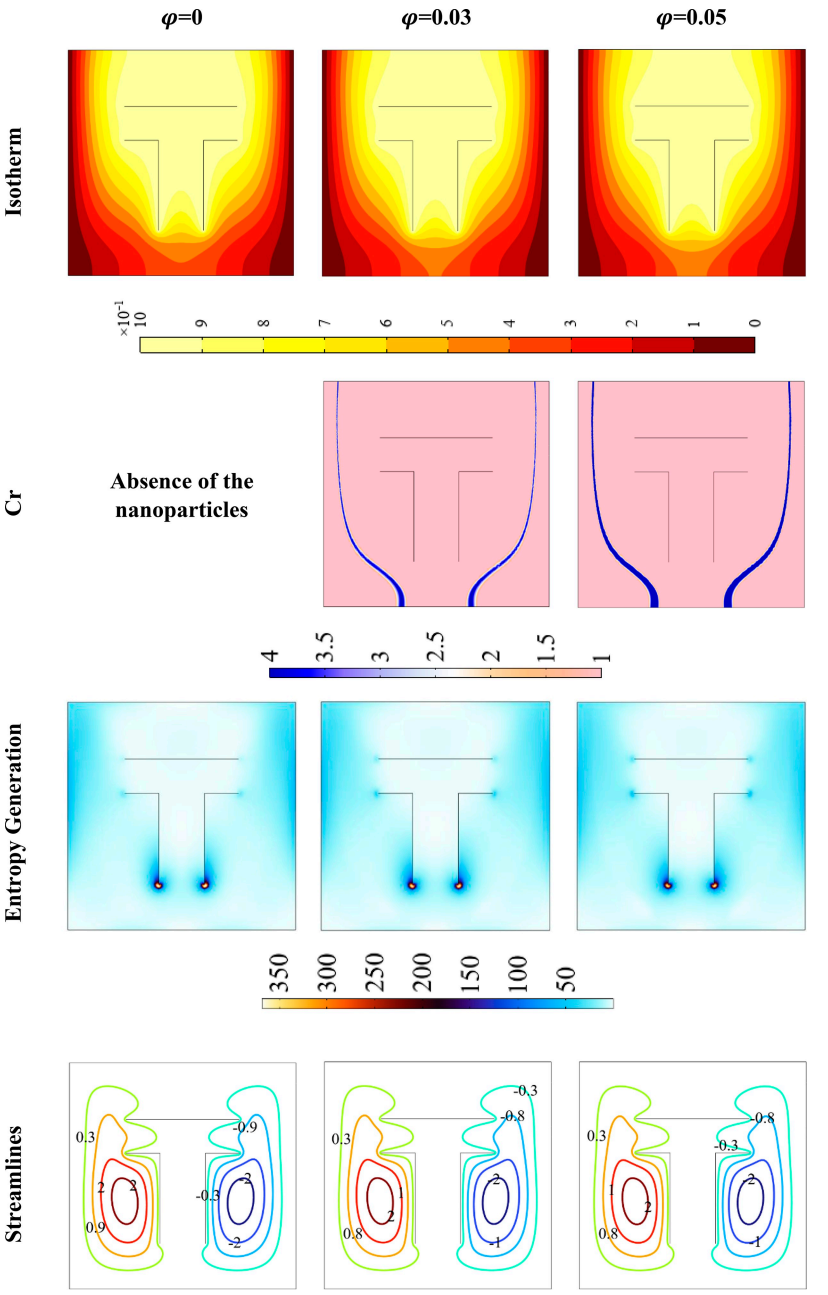

Figure 14. Influence of volume fraction of the nanoparticles (φ) on (First row) Isotherm contour, (Second row) Cr, (Third row) Entropy generation and (Fourth row) streamlines

Source: Authors' own work

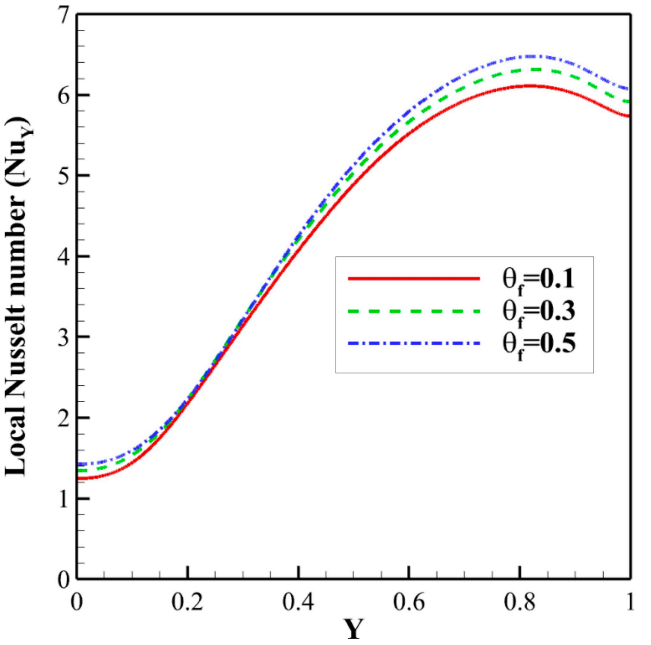

Figure 15. Influence of fusion temperature (θ_f) on Local Nusselt number
Source: Authors' own work

Table 4 presents the average Nusselt number (Nu_{avg}) and total entropy generation (S_T) for various dimensionless parameters, including aspect ratio (*AR*), Rayleigh number (Ra), nanoparticle volume fraction (φ) and fusion temperature (θ_f). These parameters are key in analyzing the thermal and flow performance of NEPCM-based systems. The data offers insights into how geometric, thermal and material properties influence heat transfer and irreversibility (entropy generation) within the system.

Starting with the aspect ratio (*AR*), the table shows that as *AR* rises from 0.05 to 0.2, the average Nusselt number rises from 4.12 to 4.50, representing an overall increase of approximately 9%. This indicates that a taller or more extended geometry improves convective heat transfer. Similarly, the total entropy generation increases from 10.18 to 11.51, about a 13% rise, reflecting greater thermodynamic irreversibility due to enhanced thermal activity across the domain. These trends suggest that optimizing the aspect ratio can moderately improve heat transfer performance but also slightly increase entropy losses.

For the Rayleigh number (Ra), the influence is much more pronounced. As Ra increases from 5,000 to 50,000, the average Nusselt number jumps from 3.87 to 7.23, marking an approximate 87% improvement. This strong increase highlights the critical role of natural convection, as higher Ra numbers intensify buoyancy-driven flows, enhancing heat transport significantly. Meanwhile, entropy generation rises dramatically from 8.50 to 37.87, about a 345% increase, indicating that while heat transfer improves substantially, it comes at the cost of much higher irreversibility. This trade-off underscores the importance of balancing thermal performance and entropy production in high-Ra systems.

The volume fraction of nanoparticles (φ) shows a more moderate effect. Increasing φ from 0 (pure fluid) to 0.05 leads to a rise in the average Nusselt number from 3.82 to 4.41,

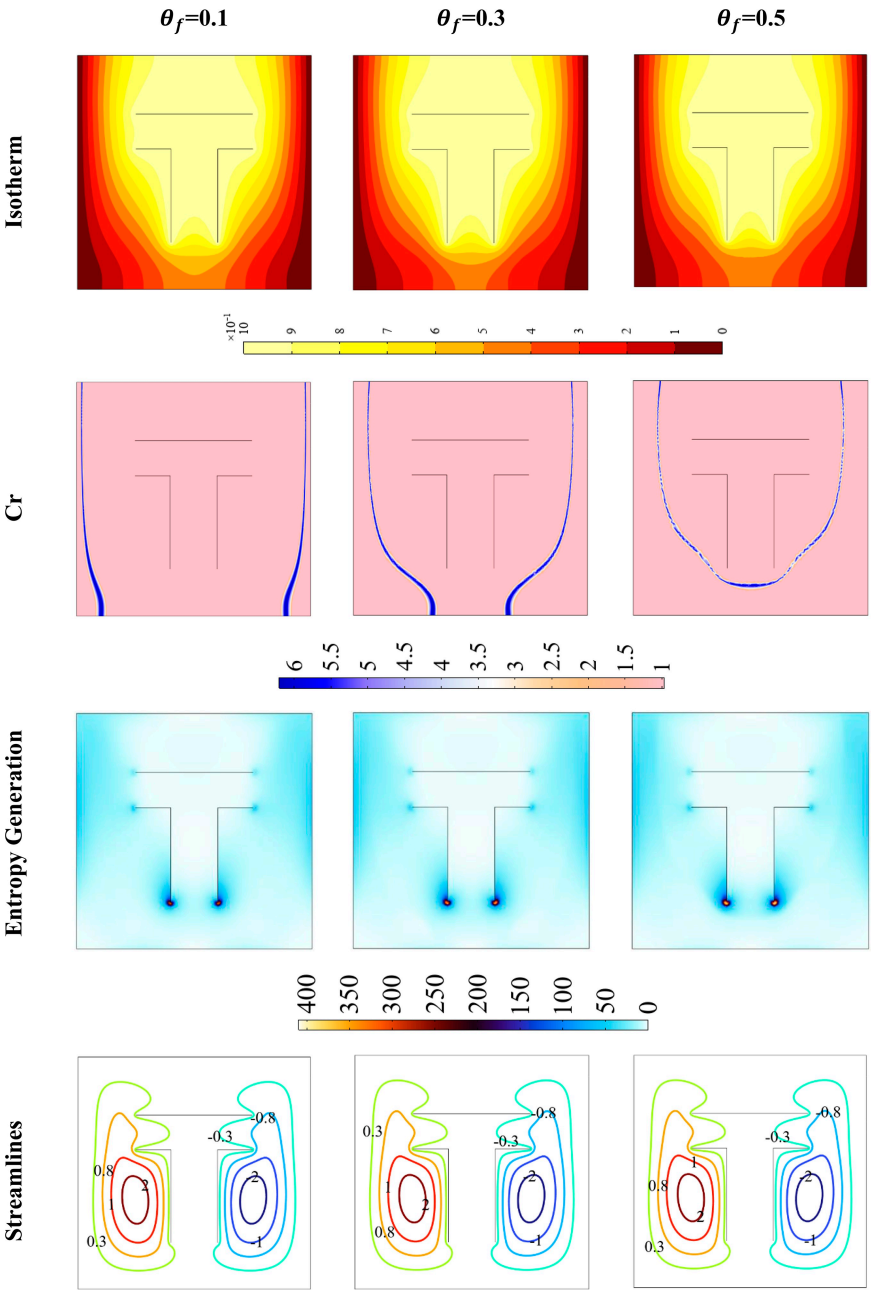

Figure 16. Impact of fusion temperature (θ_f) on (First row) Isotherm contour, (Second row) Cr, (Third row) Entropy generation and (Fourth row) streamlines

Source: Authors' own work

Table 4. Average Nusselt number and total entropy generation for different values of the nondimensional numbers and parameters

Nondimensional number/parameter	Average Nusselt number (Nu_{avg})	Total entropy generation (S_T)
Aspect ratio (*AR*)		
0.05	4.12	10.18
0.1	4.28	10.72
0.15	4.41	11.17
0.2	4.50	11.51
Rayleigh number (*Ra*)		
5,000	3.87	8.50
10,000	4.41	11.17
50,000	7.23	37.87
Volume fraction of the nanoparticles (φ)		
0	3.82	10.22
0.03	4.17	10.79
0.05	4.41	11.17
Fusion temperature (θ_f)		
0.1	4.28	10.96
0.3	4.41	11.17
0.5	4.50	11.24

Source(s): Authors' own work

about a 15% improvement. This enhancement is mainly due to the improved thermal conductivity and latent heat effects provided by the NEPCM particles, which facilitate better local heat transfer. The entropy generation also increases from 10.22 to 11.17 (approximately 9%), reflecting a modest rise in system irreversibility. These results highlight that even small additions of nanoparticles can measurably improve thermal performance with only a slight penalty in entropy generation.

Finally, the fusion temperature (θ_f) of NEPCM particles shows a relatively small but consistent impact. As θ_f increases from 0.1 to 0.5, the average Nusselt number increases from 4.28 to 4.50, an approximate 5% improvement. This suggests that higher fusion temperatures shift the phase change zone closer to the hot walls, reinforcing local temperature gradients and enhancing heat transfer. The associated entropy generation rises from 10.96 to 11.24, about a 3% increase, indicating minimal added irreversibility. Therefore, adjusting the fusion temperature serves as a fine-tuning parameter to optimize heat transfer without significantly affecting entropy production.

5. Conclusion

The heat and mass transfer characteristics of NEPCM (nanoencapsulated phase change material) suspensions within a cavity containing T-shaped internal hot walls were systematically investigated. As the NEPCM particles circulate within the suspension, they undergo phase transitions – melting and solidification – allowing them to absorb and release latent heat. This thermal storage capability significantly enhances heat transfer performance and makes NEPCM suspensions highly attractive for applications requiring efficient temperature regulation. In addition to thermal analysis, the study also examined the entropy generation associated with the NEPCM suspension, offering insights into thermodynamic

irreversibility within the system. The governing equations describing fluid flow, energy transport and phase change behavior were nondimensionalized to facilitate generalization and parameter studies. These equations were then numerically solved using the finite element method, ensuring accurate resolution of the complex flow and thermal fields. The principal conclusions drawn from this investigation are summarized as follows:

- Increasing the aspect ratio from 0.05 to 0.2 led to a 9% increase in the average Nusselt number (from 4.12 to 4.50), indicating enhanced convective heat transfer due to a longer heated surface area near the bottom of the cavity. Simultaneously, total entropy generation increased by approximately 13% (from 10.18 to 11.51), primarily due to intensified thermal activity in the lower region. Local improvements in heat transfer were most significant near the bottom of the cold wall, while effects on the upper wall remained minimal due to reduced temperature gradients.
- The Rayleigh number exhibited the most substantial impact. Raising Ra from 5,000 to 50,000 nearly doubled the average Nusselt number – from 3.87 to 7.23, an 87% increase – highlighting the dominant role of buoyancy-driven convection. However, this improvement came at the cost of a sharp increase in entropy generation, which rose from 8.50 to 37.87 (a 345% increase). The enhanced heat transfer was accompanied by distorted isotherms, a downward shift of phase transition zones and more active flow circulations.
- Increasing φ from 0 to 0.05 improved the average Nusselt number by approximately 15% (from 3.82 to 4.41), attributable to improved thermal conductivity and latent heat effects from the NEPCM particles. Entropy generation increased modestly by about 9% (from 10.22 to 11.17). Despite these enhancements, streamline patterns were largely unaffected, indicating minimal influence on overall flow structure.
- As the fusion temperature increased from 0.1 to 0.5, the average Nusselt number rose slightly, from 4.28 to 4.50 (∼5% increase), due to the repositioning of the phase change zone closer to the hot walls. Entropy generation saw a minor rise of approximately 3% (from 10.96 to 11.24). These changes occurred with minimal alteration to the flow field, confirming that the primary impact of fusion temperature is thermal rather than hydrodynamic.

References

Abderrahmane, A., Laidoudi, H., Belazreg, A. and Younis, O. (2024a), "Magneto-convection flow of nano-encapsulated phase change material (NEPCM) confined within a trapezoidal porous enclosure", *International Journal of Thermofluids*, Vol. 24, p. 100828.

Abderrahmane, A., Qasem, N.A., Belazreg, A., Khetib, Y., Younis, O., Guedri, K. and Mahariq, I. (2024b), "Convection flow of nano-encapsulated phase change material in wavy chamber with double sliding walls, flame-shaped heating source, and magnetic force", *Case Studies in Thermal Engineering*, Vol. 56, p. 104250.

Aissa, A., Belazreg, A., Laidoudi, H., Mohammed, S., Younis, O. and Alazzam, A. (2024), "Enhanced heat transmission in a triangular enclosure with a rotating cooled wall using Nano-Encapsulated phase change material nanofluid under mixed convection", *Case Studies in Thermal Engineering*, Vol. 54, p. 103992.

Alazzam, A., Qasem, N.A., Aissa, A., Abid, M.S., Guedri, K. and Younis, O. (2023), "Natural convection characteristics of nano-encapsulated phase change materials in a rectangular wavy enclosure with heating element and under an external magnetic field", *Journal of Energy Storage*, Vol. 57, p. 106213.

Alhashash, A. and Saleh, H. (2024), "Impact of convection and rotation on advanced thermal energy storage using nanoencapsulated phase change materials in wavy enclosures", *International Journal of Energy Research*, Vol. 2024 No. 1, p. 7408024.

Alhejaili, W. and Aly, A.M. (2024), "Artificial intelligence and numerical simulations for Cattaneo–Christov heat and mass fluxes of Nano-encapsulated phase change materials in a zigzag porous cavity", *Journal of Energy Storage*, Vol. 90, p. 111750.

Alsedais, N., Mansour, M.A. and Aly, A.M. (2025a), "XGBoost predictions of heat generation in MHD natural convection of hybrid nanofluid in a wavy porous cavity", *Brazilian Journal of Physics*, Vol. 55 No. 3, pp. 1-29.

Alsedais, N., Mansour, M.A., Aly, A.M. and Abdelsalam, S.I. (2025b), "Artificial neural network validation of MHD natural bioconvection in a square enclosure: entropic analysis and optimization", *Acta Mechanica Sinica*, Vol. 41 No. 9, p. 724507.

Aly, A.M. and Ahmed, S.E. (2022), "Improved incompressible SPH method for natural-convection from heated T-open pipe of Al2O3-water nanofluid in a cavity: Buongiorno's two-phase model", *Thermal Science*, Vol. 26 No. 1 Part B, pp. 613-627.

Aly, A.M. and Alsedais, N.S. (2025), "Heat and mass transfer in wavy star-shaped cavities with nano-enhanced phase change material: numerical simulation and machine learning applications", *International Journal of Numerical Methods for Heat and Fluid Flow*, Vol. 35 No. 4.

Aly, A.M., Huang, C. and Alotaibi, M. (2025), "Study on heat and mass transfer in a porous cavity based on artificial intelligence δ-SPH model", *International Communications in Heat and Mass Transfer*, Vol. 164, p. 108907.

Aly, A.M., Hussein, A.K., Younis, O., Alsedais, N. and Kolsi, L. (2022), "Double-diffusive convection of two rods in a novel cavity saturated by porous media and suspended by Nano-encapsulated phase change materials", *Waves in Random and Complex Media*, pp. 1-25.

Barlak, S., Sara, O.N., Karaipekli, A. and YAPıCı, S. (2016), "Thermal conductivity and viscosity of nanofluids having nanoencapsulated phase change material", *Nanoscale and Microscale Thermophysical Engineering*, Vol. 20 No. 2, pp. 85-96.

Calcagni, B., Marsili, F. and Paroncini, M. (2005), "Natural convective heat transfer in square enclosures heated from below", *Applied Thermal Engineering*, Vol. 25 No. 16, pp. 2522-2531.

Chai, L., Shaukat, R., Wang, L. and Wang, H.S. (2018), "A review on heat transfer and hydrodynamic characteristics of nano/microencapsulated phase change slurry (N/MPCS) in mini/microchannel heat sinks", *Applied Thermal Engineering*, Vol. 135, pp. 334-349.

Chen, B., Wang, X., Zeng, R., Zhang, Y., Wang, X., Niu, J., Li, Y. and DI, H. (2008), "An experimental study of convective heat transfer with microencapsulated phase change material suspension: laminar flow in a circular tube under constant heat flux", *Experimental Thermal and Fluid Science*, Vol. 32 No. 8, pp. 1638-1646.

Ghalambaz, M., Sheremet, M.A. and Pop, I. (2015), "Free convection in a parallelogrammic porous cavity filled with a nanofluid using Tiwari and Das' nanofluid model", *Plos One*, Vol. 10 No. 5, p. e0126486.

Ghalambaz, M., Chamkha, A.J. and Wen, D. (2019), "Natural convective flow and heat transfer of nano-encapsulated phase change materials (NEPCMs) in a cavity", *International Journal of Heat and Mass Transfer*, Vol. 138, pp. 738-749.

Ghalambaz, M., Jin, H., Bagheri, A., Younis, O. and Wen, D. (2022), "Convective flow and heat transfer of nano-encapsulated phase change material (NEPCM) dispersions along a vertical surface", *Facta Universitatis, Series: Mechanical Engineering*, Vol. 20 No. 3, pp. 519-538.

Ghalambaz, M., Mozaffari, M., Yazdani, S., Abbaszadeh, M., Sheremet, M. and Ghalambaz, M. (2023), "Conjugate entropy generation and heat transfer of a dilute suspension of nano-encapsulated phase change material in a partially heated wall cavity", *Reports in Mechanical Engineering*, Vol. 4 No. 1, pp. 175-192.

Ghalambaz, M., Pop, I., Sheremet, M., Ali, M.H. and Ghalambaz, M. (2024a), "Numerical and artificial neural network analysis of magnetohydrodynamic natural convection in a nano-encapsulated phase change suspension filled quadrantal circular enclosure", *Journal of Applied and Computational Mechanics*, Vol. 11 No. 4, pp. 929-945.

Ghalambaz, M., Yusaf, T., Pop, I., Shafi, J., Baro, M. and Fteiti, M. (2024b), "Magnetohydrodynamic free convection of nano-encapsulated phase change materials between two square cylinders: mapping the thermal behavior using neural networks", *Alexandria Engineering Journal*, Vol. 89, pp. 110-124.

Hidki, R., EL Moutaouakil, L., Boukendil, M., Charqui, Z. and Jamal, B. (2024), "Application of an artificial intelligence model for natural convection of nano-encapsulated phase change materials (NEPCMs) confined in a porous square enclosure with an inclined elliptical heated block", *International Communications in Heat and Mass Transfer*, Vol. 155, p. 107546.

Ilis, G.G., Mobedi, M. and Sunden, B. (2008), "Effect of aspect ratio on entropy generation in a rectangular cavity with differentially heated vertical walls", *International Communications in Heat and Mass Transfer*, Vol. 35 No. 6, pp. 696-703.

Kahveci, K. (2010), "Buoyancy driven heat transfer of nanofluids in a tilted enclosure", *Journal of Heat Transfer*, Vol. 132 No. 6, p. 62501.

Khanafer, K. and Vafai, K. (2011), "A critical synthesis of thermophysical characteristics of nanofluids", *International Journal of Heat and Mass Transfer*, Vol. 54 Nos 19-20, pp. 4410-4428.

Khedher, N.B., Aljibori, H.S.S., Mehryan, S., Hajjar, A., Ghalambaz, M., Boujelbene, M., Elbashir, N. B. and Mahariq, I. (2024a), "Vibrational convection in thermal systems: Nano-encapsulated phase change material in a porous enclosure", *International Communications in Heat and Mass Transfer*, Vol. 157, p. 107719.

Khedher, N.B., Mehryan, S., Hajjar, A., Alghawli, A.S., Ghalambaz, M., Ayoubloo, K.A. and Dhahbi, S. (2024b), "Optimizing heat flow: nano-encapsulated phase change materials in vibration-enhanced gravity-driven thermal convection", *International Communications in Heat and Mass Transfer*, Vol. 151, p. 107212.

Mourad, A., Hocine, N., Abderrahmane, A., Younis, O. and Marzouki, R. (2025), "Double diffusion heat convection of a porous enclosure loaded with nano-encapsulated phase change materials", *International Communications in Heat and Mass Transfer*, Vol. 163, p. 108764.

Raizah, Z. and Aly, A.M. (2022), "A rotating superellipse inside a hexagonalshaped cavity suspended by nano-encapsulated phase change materials based on the ISPH method", *International Journal of Numerical Methods for Heat and Fluid Flow*, Vol. 32 No. 3, pp. 956-977.

Reddy, P. and Sreedevi, P. (2024), "Enhanced entropy generation and heat transfer characteristics of magnetic nano-encapsulated phase change materials in latent heat thermal energy storage systems", *Applied Mathematics and Mechanics*, Vol. 45 No. 6, pp. 1051-1070.

Reddy, P.S., Sreedevi, P. and Ghalambaz, M. (2024), "Heat transfer investigation of nano–encapsulated phase change materials (NEPCMs) in a thermal energy storage device", *Applied Thermal Engineering*, Vol. 250, p. 123495.

Suchana, K. and Molla, M.M. (2024), "Magnetohydrodynamic double diffusion natural convection of power-law Non-Newtonian Nano-Encapsulated phase change materials in a trapezoidal enclosure", *International Journal of Numerical Methods for Heat and Fluid Flow*, Vol. 34 No. 10, pp. 3764-3792.

Turan, O., Sachdeva, A., Chakraborty, N. and Poole, R.J. (2011), "Laminar natural convection of power-law fluids in a square enclosure with differentially heated side walls subjected to constant temperatures", *Journal of Non-Newtonian Fluid Mechanics*, Vol. 166 Nos 17-18, pp. 1049-1063.

Vemula, R. and Öztop, H.F. (2024), "Heat transfer in a non-uniformly heated enclosure filled by NEPCM water nanofluid", *International Journal of Numerical Methods for Heat and Fluid Flow*, Vol. 34 No. 12, pp. 4384-4408.

Wang, W., Jin, Y.-H., Chen, Y.-M., Hu, Z.-M., Zhou, R.-R., Tian, H., Xin, F. and Li, X.-Z., (2024), "Hydrothermal and entropy generation analyses of natural convection of nano-encapsulated phase change materials suspension in a cavity subjected to the localized heating", *Journal of Energy Storage*, Vol. 77, p. 109865.

Zaraki, A., Ghalambaz, M., Chamkha, A.J., Ghalambaz, M. and DE Rossi, D. (2015), "Theoretical analysis of natural convection boundary layer heat and mass transfer of nanofluids: effects of size, shape and type of nanoparticles, type of base fluid and working temperature", *Advanced Powder Technology*, Vol. 26 No. 3, pp. 935-946.

Zienkiewicz, O.C., Taylor, R.L. and Nithiarasu, P. (2014), "The finite element method for fluid dynamics", in Zienkiewicz, O.C., Taylor, R.L. and Nithiarasu, P. (Eds), *The Finite Element Method for Fluid Dynamics*, 7th ed., Butterworth-Heinemann, Oxford.

Corresponding author
Ioan Pop can be contacted at: ipop@math.ubbcluj.ro